LAWRENCE
LIVERMORE
NATIONAL
LABORATORY

UCRL-JRNL-221815

# Radial Particle Flux in the SOL of DIII-D During ELMing H-Mode

A. W. Leonard, J. A. Boedo, M. Groth, B. L. Lipschultz, G. D. Porter, D. L. Rudakov, D. G. Whyte

June 4, 2006

Journal of Nuclear Materials

## Disclaimer

# Radial particle flux in the SOL of DIII-D during ELMing H-mode

**A.W. Leonard**[a*], J.A. Boedo[b], M. Groth[c], B.L. Lipschultz[d], G.D. Porter[c], D.L. Rudakov[b], D.G. Whyte[e]

[a]*General Atomics, P.O. Box 85608, San Diego, California 92186-5608, USA*

[b]*University of California-San Diego, La Jolla, California, USA*

[c]*Lawrence Livermore National Laboratory, Livermore, California, USA*

[d]*Massachusetts Institute of Technology, Cambridge, Massachusetts, USA*

[e]*University of Wisconsin, Madison, Wisconsin, USA*

**Abstract.** The radial particle flux in the scrape-off-layer (SOL) during ELMing H-mode is examined in DIII-D as a function of density. The global radial particle flux in the outboard far SOL is determined by a window frame technique. Between ELMs the outboard far SOL particle flux increases strongly with density but remains similar to the particle flux across the separatrix as estimated by the pedestal density and temperature gradients. At low density the steep density gradient of the pedestal extends up to 2 cm outside the separatrix. At high density the density gradient flattens just outside the separatrix making this region critical for assessment of the far SOL particle flux. During ELMs the far SOL particle flux becomes localized to the outboard midplane and the assumptions for the window frame analysis break down. Implications for scaling of main chamber wall particle flux and pedestal fueling are explored.

*Journal of Nuclear Materials Keywords*: P0600, P0500

*PSI-17 Keywords*: Particle flux, Cross-field transport, Recycling, DIII-D, ELMs

*PACs*: 52.55.Fa, 52.25.Fi

*Corresponding and presenting author*: A.W. Leonard, General Atomics, P.O. Box 85608, San Diego, California 92186-5608, e-mail: Leonard@fusion.gat.com

## 1. Introduction

Particle flux to plasma facing components is largely responsible for the generation of impurities in the plasma, and its distribution can affect plasma flow and fueling of the pedestal. Several studies have examined the contributions of scrape-off layer (SOL) radial particle transport in the main chamber to the overall surface particle flux in DIII-D [1-5]. Radial transport in the far SOL can be large and convective in nature, dominated by intermittent transport events, leading to significant particle flux to the main chamber, particularly at high density [3,4]. While many of these studies have examined L-mode, some data in H-mode with edge localized modes (ELMs) indicate that the wall flux at the outboard midplane can be dominated by the particle flux during ELMs, particularly at low density [5]. Detailed comparison of modeling and data of the 2D recycling profile in DIII-D at low density $\left(n_e/n_{GW} \sim 0.3\right)$ indicates that the pedestal can still be largely refueled from the divertor region [6].

This study examines the consistency of the previous measurements and their implications for global particle flux in the context of ELMing H-mode as a function of density. The particle flux across the separatrix is compared to fluxes to the outboard main chamber and the divertor target, with the fluxes between ELMs and during ELMs treated separately.

## 2. Experimental Setup

This experimental study was carried out in a lower single null discharge as shown in Fig. 1. These discharges were run with a plasma current of 1.0 MA, and a toroidal field of 1.7 T for a $q_{95}$ of ~4.3. The neutral beam injected power remained constant at 4.8 MW. The density was scanned on shot by shot basis by a combination of divertor pumping and external gas puffing. The density scan achieved a range of pedestal density from $2.5\text{-}6.4\times10^{19}$ $m^{-3}$, or $n_{e,ped}/n_{Greenwald(GW)} \sim$ 25%-65%. The Type I ELMs maintained a constant frequency of

about 80 Hz over this density range, though there was considerably more large scale fluctuations in the midplane $D_\alpha$ signals between ELMs at the higher density.

The diagnostics used for this study are also shown in Fig. 1. Thomson scattering is used for pedestal and near SOL profiles. In order to obtain Thomson measurements farther out into the SOL at low density, the Thomson pulses over a time window are sorted with respect to the ELM phase. The photons from multiple laser pulses for each 20% of the ELM period are then added and analyzed for a single profile. Typical electron density and temperature profiles from the density scan are shown in Fig. 2. The far SOL plasma is measured with an insertable Langmuir probe, also shown in Fig. 1. The probe makes two plunges each shot to a radius on the same flux surface as the corner of the upper baffle, a toroidally symmetric surface. Typical profiles from the probe at low and high density are also shown in Fig. 2. The insertable probe measurements are also compared with a fixed Langmuir probe on the upper baffle and probes on the lower divertor target.

### 3. Separatrix particle flux

The steady particle flux across the separatrix can be estimated by examining the edge density and temperature gradients. In a previous study on DIII-D [7] it was found, by examining the density rise just after the H-mode transition, that the particle diffusivity, $D_\perp$, in the pedestal is roughly 25%±10% of the thermal diffusivity, $\chi_{eff}$, over a range of conditions. To carry out this analysis for the density scan shown in Fig. 2, the profiles were first fit with a tanh function. With the separatrix location set at the foot of the temperature fit, $\chi_{eff}$ is determined from the $T_e$ gradient at that location and the radial energy flux is assumed to be 70% of the injected power to account for radiation and ELM losses. The variation of radiation plus ELM loss is not expected to be large over the density scan. The global separatrix particle flux is then calculated from the density gradient assuming $D_\perp = 25\%$ of $\chi_{eff}$. The resultant separatrix particle flux between ELMs from this analysis, shown in Fig. 3, is approximately

500 amperes of deuterium ions at low density and rises to about 1.5 kA at the higher densities of this scan. The increase in particle current at high density is primarily due to an increased $\chi_{eff}$ and implied increased $D_{\perp}$. The particle flux across the separatrix that occurs intermittently during ELMs is also significant and can be calculated by comparing the density profile just before and just after an ELM. A time dependent density profile is constructed by sorting the Thomson density profiles with respect to the ELM phase in a time window of otherwise constant conditions [8]. The reconstructed profiles, just before and just after the ELM, are integrated and the difference represents the particle lost at an average ELM. The single ELM particle loss multiplied by the ELM frequency then determines the time-averaged particle flux during ELMs. This analysis was performed for the density scan with the resulting separatrix flux also plotted in Fig. 3. The ELM flux is similar to the flux between ELMs at low density, ~500 A, but rises only slightly at higher density. The relatively constant time-averaged ELM particle flux is not surprising given that the ELM frequency is not changing significantly with density.

## 4. Far SOL particle flux

In the far SOL the global radial particle flux to the outboard main chamber is estimated by a "window frame" analysis [1]. This analysis determines the particle flux through the magnetic flux surface marked with the dashed line in Fig. 1, 4 cm from the outboard midplane separatrix. An important feature of this surface is that both ends of the field lines terminate on a toroidally symmetric surface. This analysis assumes parallel plasma flow to the surface with negligible recycling in the low-density far SOL plasma. Under these conditions the particle flux through the window frame is given by, [Ref. 1]

$$\Gamma_i = 2\pi n_e c_s \lambda_n \frac{B_p}{B_T} \left[ (\langle R \rangle \xi)_1 + (\langle R \rangle \xi)_2 \right] \quad . \tag{1}$$

Where $n_e$, $c_s$, $\lambda_n$, are density and sound speed and their convoluted e-folding scale length measured by the midplane probe, and $B_p$ and $B_T$ are the midplane windowframe values of toroidal and poloidal magnetic field respectively. Also $R$ is the average major radius of the upper and lower halves of the window frame flux surface and $\xi$ is the ratio of saturation current between the termination surfaces and the midplane, ~0.5. More details and assumptions of this analysis can be found in Ref. [1].

Typical profiles between ELMs in the SOL from the midplane probe, and Thomson scattering mapped to the midplane, are shown in Fig. 2. The gaps in the probe profiles are due to the removal of ELMs. The probe data is generally in good agreement with the Thomson data in regions of overlap. To determine the midplane window frame plasma conditions, the probe profiles of electron density and temperature, and ion saturation current ($I_{sat}$) are all fit to an exponential function from the window frame radius outward, in the shadow of the baffle limiters. The midplane window frame density increases continuously from $1.0\times10^{18}$ $m^{-3}$ to $3.5\times10^{18}$ $m^{-3}$ across the pedestal density scan of 2.5-6.4$\times10^{19}$ $m^{-3}$. The electron temperature remains roughly constant with density at 15 eV. The midplane scale lengths also reflect this trend with the density and $I_{sat}$ scale length increasing from 1 cm to 4 cm across the density scan while temperature scale length remains constant at roughly 5 cm.

The between ELM window frame particle flux calculated from the midplane measurements, using the $I_{sat}$ measurements from the probe directly for the factors $n_e c_s$ and $\lambda$, are shown in Fig. 4. The separatrix fluxes between ELMs are also shown for reference. Though somewhat less at low density, overall the window frame flux between ELMs is roughly equal to the separatrix flux between ELMs. As a cross check of this analysis the window frame flux implied by measurements of a fixed Langmuir probe in the upper baffle, Fig. 1, are also plotted in Fig. 4. The baffle radial flux is calculated from the baffle probe saturation current and an assumed falloff length consistent with the midplane measurements,

and is thus a cross check of the window frame analysis assumptions. At low density the baffle probe saturation current is near the measurement resolution and systematic effects, such as a voltage offset, could result in the somewhat lower baffle flux than implied by the midplane measurements. At high density the baffle probe saturation current is higher than the midplane probe and may indicate the window frame analysis is beginning to break down with local recycling.

While the flux between ELMs is a factor 2-3 smaller than the L-mode flux of previous studies at the same line averaged density [1,2], due to the pedestal transport barrier, the flux increases with density in both L-mode and H-mode in a similar manner. Also consistent with the previous L-mode results, a radial convective velocity of ~100 m/s could account for the observed window frame flux. This study finds the density scale length outside the window frame surface in H-mode to increase with density. Previous L-mode studies have found either a constant scale length [1] or an increasing scale length [5]. The same analysis as above can potentially be applied for the outboard main chamber particle flux during ELMs. Though there is large variation in the midplane probe density across an ELM, averaging over the first quarter of the ELM cycle produces reasonable agreement in the region of overlap with the averaged Thomson data. At the midplane, the density is much more affected than the electron temperature by the ELM. This is consistent with previous DIII-D ELM measurements that showed the ELM $T_e$ perturbation decays much more quickly in the SOL than the ELM $n_e$ perturbation [9]. While the window frame $T_e$ scale length does not change significantly at an ELM, the $n_e$ scale length does rise to approximately that of $T_e$.

Before calculating the global outboard ELM flux the assumptions of the window frame analysis should be tested. In Fig. 5 the baffle probe ion saturation current is compared to the midplane probe current on the same flux surface. The observation that the midplane current is more than a factor of two greater than the baffle current indicates that the window frame

assumptions are no longer valid. This comparison indicates the ELM flux is highly localized to the midplane. A localized midplane flux could result from strong asymmetries and localizations of the ELM perturbation, or a midplane radial velocity of the ELM faster than the parallel equilibration time along a flux tube. Though it is not possible to determine the global outboard flux due to ELMs, the relative contribution of ELMs to the midplane flux can be estimated by comparing the time-averaged probe saturation current during ELMs to between ELMs. Using this analysis the ELMs represent ~80% of the total midplane flux at low density, decreasing to ~60% at the higher densities. This is consistent with a previous measurement that showed the particle flux to the outboard midplane wall was dominated by the ELM flux at low density, but became comparable to the between ELM flux at higher densities [5].

## 5. Discussion

The density profiles in Fig. 2 exhibit qualitative differences with increasing density. In the pedestal, inside the separatrix, the density scale lengths remain similar with increasing density. Outside the separatrix at low density, the density scale length remains small up to 2 cm outside the separatrix before increasing in the far SOL. At high density, the scale length increases significantly just outside the separatrix and remains constant throughout the SOL to the outboard window frame to the midplane wall. The short scale length outside the separatrix at low density is an indication that the transport barrier can extend beyond the separatrix. Beyond this region at low density, and throughout the SOL in high density, the flatter profiles indicate the stronger radial transport observed previously in L-mode is active, with a similar effective convective velocity, ~100 m/s. Understanding what sets the width of the steep density gradient outside the separatrix will be required for assessing main chamber particle flux in future large tokamaks.The main chamber particle flux during ELMs is also significant. At the midplane particle flux is dominated by ELMs particularly at low density, as has been

observed in a previous study [5]. The analysis of Fig. 5 indicates that the ELM flux is poloidally localized to the midplane, with a factor of 5, or more, greater flux than to outboard upper baffle. Further details of the ELM particle wall deposition will require more localized measurements around the periphery of the outboard main chamber.

For fueling of the pedestal from main chamber, the contribution from ELMs can be separated from the flux between ELMs because of the short ELM time scale. The decay of the midplane $D_\alpha$ ~ 1 ms, signal is much faster than the ELM period, ~15 ms. Between ELMs the flux to the outboard window frame is roughly equal to the particle flux across the separatrix, Fig. 4. The total divertor flux, from fixed divertor Langmuir probe measurements, is roughly 10 times this value, in line with previous L-mode observations [1]. Most of the outboard main chamber particle flux will recycle off the upper and lower baffles, Fig. 1, since the midplane separatrix to wall distance is much greater than the density decay length. A rough estimate using an isotropic distribution of Frank-Condon neutrals recycled from the baffles indicates that significantly less than half are likely to cross the separatrix before ionization in the SOL at low density. An even smaller fraction should penetrate the separatrix at high density. The divertor flux, while 10 times the window frame flux, faces a denser plasma and greater likelihood of ionization before fueling the pedestal. While an earlier study of low density H-mode found that the divertor surface particle flux could account for the observed pedestal fueling [6], the main chamber particle source was not considered. A detailed 2D analysis of the edge plasma and neutrals is needed to quantify the relative contributions of the outboard main chamber and divertor to pedestal fueling.

## 6. Conclusions

The radial particle flux through the separatrix and the outboard far SOL have been measured by a variety of techniques in ELMing H-mode. Between ELMs the outboard main chamber particle flux is roughly equal to the flux across the separatrix, both increasing strongly with increasing core plasma density. At low density the steep density gradient extends up to 2 cm outside the separatrix, while at high density the profile flattens just outside the separatrix. The flux to the divertor target is about 10 times larger than to the outboard main chamber, but further edge plasma analysis and modeling is required to assess the relative contributions to pedestal fueling. About half the particle flux across the separatrix occurs during ELMs at low density with a smaller fraction at high density where the turbulent transport between ELMs increases. The radial particle flux during ELMs is preferentially localized to the outboard midplane. This results in the midplane particle flux being dominated by the ELMs.

## Acknowledgment

This work was supported by the U.S. Department of Energy under DE-FC02-04ER54698, DE-FC02-04ER54758, W-7405-ENG-48 (with UC, LLNL), DE-FC02-04ER54762, and DE-FG03-01ER54615.

**References**

[1] D.G. Whyte, B.L. Lipschultz, P.C. Stangeby et al., Plasma Phys. Control. Fusion **47** (2005) 1579.

[2] B. Lipschultz, D. Whyte and B. LaBombard, Plasma Phys. Control. Fusion **47** (2005) 1559.

[3] J.A. Boedo, D.L. Rudakov, R.A. Moyer, et al., Phys. Plasmas **10** (2003) 1670.

[4] J.A. Boedo, D.L. Rudakov, R.J. Colchin, et al., J. Nucl. Mater. **313-316** (2003) 813.

[5] D.L. Rudakov, J.A. Boedo, R.A. Moyer, et al., Nucl Fusion **45** (2005) 1589.

[6] M. Groth, L.W. Owen, G.D. Porter, et al., J. Nucl. Mater. **337-339** (2005) 425.

[7] G.D. Porter, Phys. Plasmas **5** (1998) 4311.

[8] A.W. Leonard, T.H. Osborne, M.E. Fenstermacher, et al., Phys. Plasmas **10** (2003) 1765.

[9] J.A. Boedo, D.L. Rudakov, E. Hollmann, et al., Phys. Plasmas **12** (2005) 072516.

**List of Figures**

Fig. 1. (a) The diagnostics and magnetic configuration used in this study. Shown are the edge Thomson scattering, a fixed upper baffle Langmuir probe, the midplane insertable Langmuir probe, the edge tangential $D_\alpha$ array and the lower divertor Langmuir probes. Also shown is the magnetic surface used for the window frame particle flux analysis.

Fig. 2. The pedestal and edge (a) density and (b) electron temperature between ELMs from Thomson scattering and the midplane Langmuir probe. Four representative profiles from the density scan are shown for the Thomson data. A high and low density case are shown for the midplane probe.

Fig. 3. Time-averaged particle flux across the separatrix between ELMs and during ELMs.

Fig. 4. The radial particle flux between ELMs through the outboard window frame as measured by the midplane probe. Also shown are the radial fluxes implied by the upper baffle Langmuir probe assuming scale lengths measured at the midplane. Also shown for reference are the fluxes across the separatrix between ELMs from Fig. 3.

Fig. 5. The time-averaged saturation current (Amperes/$m^2$) due to ELMs from the midplane Langmuir probe and the upper baffle Langmuir probe.

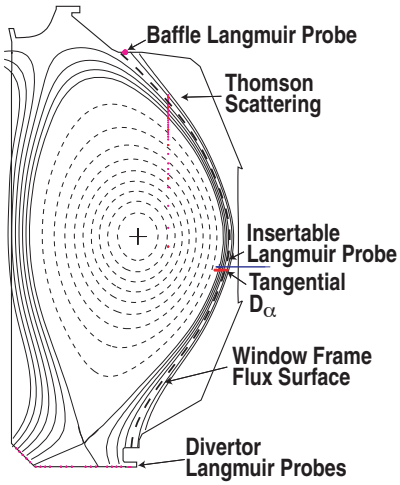


A.W. Leonard Figure 1

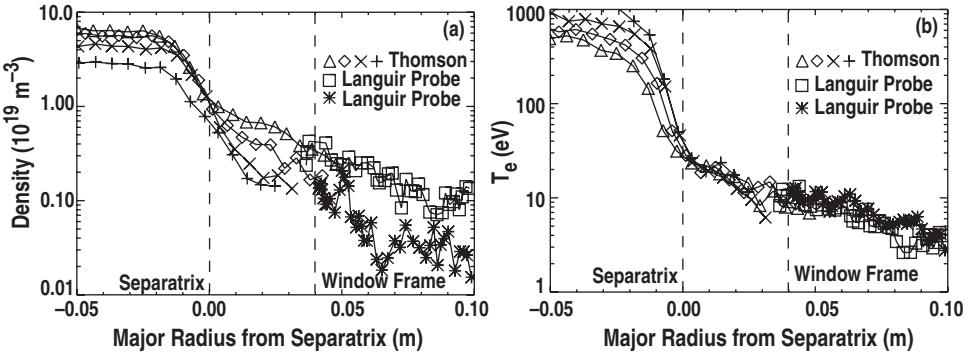


A.W. Leonard Figure 2

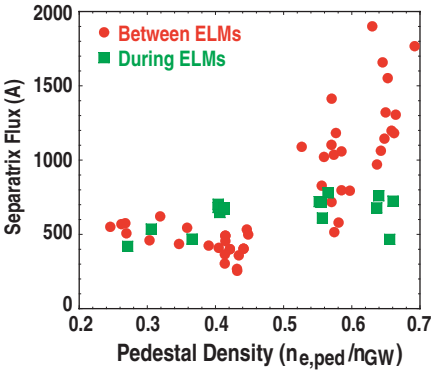


A.W. Leonard Figure 3

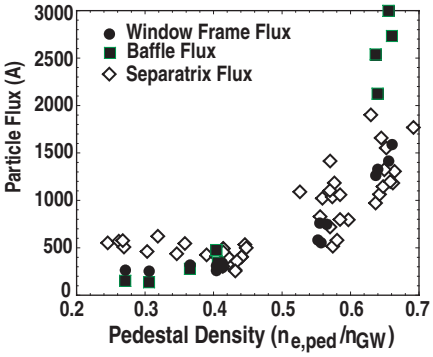


A.W. Leonard Figure 4

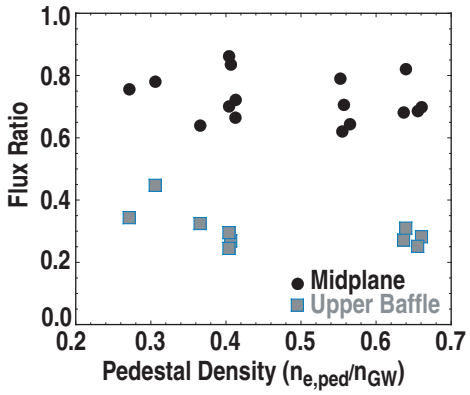


A.W. Leonard Figure 5